Lattice dielectric and thermodynamic properties of yttria stabilized zirconia solids

2009 J. Phys.: Condens. Matter 21 145402

(http://iopscience.iop.org/0953-8984/21/14/145402)

IOP Publishing Journal of Physics: Condensed Matter

J. Phys.: Condens. Matter **21** (2009) 145402 (6pp) doi:10.1088/0953-8984/21/14/145402

Lattice dielectric and thermodynamic properties of yttria stabilized zirconia solids

Kah Chun Lau[1,3] **and Brett I Dunlap**[2]

[1] Department of Chemistry, George Washington University, Washington, DC 20052, USA
[2] Naval Research Laboratory, Code 6189, Washington, DC 20375, USA

E-mail: kah.lau.ctr.my@nrl.navy.mil

Received 21 January 2009, in final form 11 February 2009
Published 5 March 2009
Online at stacks.iop.org/JPhysCM/21/145402

Abstract

A study of lattice dielectric and thermodynamic properties of yttria stabilized zirconia (YSZ) crystals as a function of yttria concentration is reported. This study is based on density functional perturbation theory, using ABINIT. Within the local density approximation and the harmonic approximation, we find excellent agreement between calculated and low temperature experimental specific heat and dielectric constants. From the variation of the specific heat of YSZ with the yttria composition, we propose a simple additivity rule that estimates the dependence of the specific heat of YSZ on the yttria concentration, whereas for the dielectric constants of YSZ, the values are bounded by the dielectric constants of cubic and amorphous zirconia.

(Some figures in this article are in colour only in the electronic version)

1. Introduction

Of energy conversion devices, perhaps the most promising is the solid oxide fuel cell (SOFC). It can use yttria stabilized zirconia (YSZ) as an ion conducting electrolyte membrane in high temperature operation. Compared to the ionic conductivity of bulk YSZ at high temperatures (i.e. $\sim 10^{-1}$–10^{-2} S cm^{-1} between 700 and 1000 °C), its conductivity at room temperature is negligible [1]. For the bulk YSZ, it is a solid solution on a cubic fluorite lattice with yttrium and zirconium distributed on a face-centered-cubic cation lattice and oxygen and vacancies distributed on a simple-cubic anion lattice [2]. Advancing the development of these solid state energy devices is contingent on understanding materials properties at a fundamental level. Structural and ionic conductivity can differ substantially due to different competing thermodynamic phases for varying ZrO_2–Y_2O_3 composition ratios [3]. With redistribution of mobile ionic species within the YSZ electrolyte and its contact interfaces upon operation, the build up of space-charge regions, the electrochemical double layers, within the system makes it a capacitive medium, modeled phenomenologically with equivalent circuit model [4].

Under static condition, i.e. without ionic current, the relative permittivity of a medium or the dielectric constant of a material controls the capacitive properties of that system. Thus, it is reasonable to assume that variation in relative permittivity of this capacitive medium due to yttrium concentration should affect the ionic current from this solid state electrochemical device. This assumption has been verified from our recent atomistic, yet still phenomenological, kinetic Monte Carlo simulation of a working YSZ fuel cell cathode [5]. In addition to the hole concentration due to mol% yttria (Y_2O_3) concentration and operating temperature, we found the dielectric constant (ϵ) of YSZ to be another important factor determining the ionic current through the fuel cell. The experimental ϵ values of YSZ are large and scattered between 10 and 41 at room temperature [6] due to different morphologies. However, very little guidance is available to correlate the ϵ of YSZ to different mol% Y_2O_3 concentrations. Furthermore, it is important eventually to find a general way to correlate the dielectric properties of YSZ under different yttria concentration ratios as well as under the various operating conditions of a working fuel cell. To achieve this goal ultimately, accurate quantum mechanical benchmark

[3] Author to whom any correspondence should be addressed.

calculations are a necessary first step. Thus the YSZ lattice dielectric and thermodynamic properties are our focus in this work.

2. Methodology

Density functional perturbation theory [7] is employed to compute quantities that are due entirely or in part to lattice dynamics. Our calculations are performed within the local density approximation (LDA) to density functional theory, as implemented in the ABINIT package [8]. The exchange–correlation energy is evaluated using the Perdew–Wang parameterization of Ceperley–Alder electron gas data. The all-electron potentials were replaced by the relativistic Hartwigsen–Goedecker–Hutter pseudopotentials [9] with O(2s, 2p), and Y(4s, 4p, 4d, 5s), Zr(4s, 4p, 4d, 5s) levels treated as valence states with semicore 4s and 4p states. The wavefunctions are expanded in plane waves up to a kinetic energy cutoff of 35 hartree. Integrals over the Brillouin zone (BZ) were replaced by sums on mesh of Monkhorst–Pack $4 \times 4 \times 4$ special k points [10]. Calculations were deemed converged when changes in total energy were less than 10^{-6} hartree and those in the interatomic forces were less than 10^{-5} hartree bohr^{-1} for full structural relaxation. Linear response properties are obtained as second derivatives of the total energy with respect to an external electric field or to atomic displacements, which are calculated within a variational approach to density functional perturbation theory [7, 11–13], as implemented in the ABINIT package [8]. In order to achieve convergence in the heat capacities at constant volume, C_V, a grids of $20 \times 20 \times 20$ (i.e. ZrO_2) and $10 \times 10 \times 10$ (i.e. YSZ) q points in the irreducible Brillouin zone (BZ) was employed for the evaluation of the integrals corresponding to the phonon DOS and the thermodynamic properties.

To test the accuracy of our computational parameters, the cubic (c-ZrO_2 in $Fm3m$ space group) and monoclinic (m-ZrO_2 in $P2_1/c$ space group) phases of zirconia which are well studied [2, 14–19], are chosen to benchmark our calculations. For these zirconia polymorphs, the optimized structural parameters of c-ZrO_2 and m-ZrO_2 are listed in table 1. The structural parameters match well the reported values [14, 17–19], and our total energy calculations have correctly reproduced the energetics of these two ZrO_2 phases. The difference in cohesive energies for the m-ZrO_2 and c-ZrO_2 is 0.12 eV/(ZrO_2 unit), relative to 0.10 eV/(ZrO_2 unit) from a previous LDA study [19].

3. Results and discussion

Compared to determining the geometry and energetics of competing phases of ZrO_2 polymorphs, searching for ground state atomic arrangements across a composition range of ZrO_2–Y_2O_3 is definitely more complicated. For YSZ, the inherited complexity is due to its multifaceted ordering problem. The structures and lattices are not merely determined by different composition at different ambient condition, but also dictated by intrinsic long- and short-range order in the system [20]. In normal conditions, the fluorite scaffold is expected to be stable for yttria (Y_2O_3) content in the range of ∼8–40% mol [20–24]. At lower yttria content, the cubic phase can give way to two-phase equilibria with another two zero-pressure zirconia polymorphs (i.e. t- and m-ZrO_2), and therefore the solid is inhomogeneous. For higher yttria concentration (i.e. ⩾40% mol) the system is expected to crystallize in ordered form [23]. Our aim is not to go into depth for the detailed analysis of configurational space for structural ordering and defect clustering at various compositions, instead, we focus on the phonon, dielectric and thermodynamic properties of perfect crystal lattices, based on the ground state structures suggested from previous studies [20, 23].

Table 1. Structural parameters obtained for the c-ZrO_2, m-ZrO_2, Σ-YSZ, Ω-YSZ, Φ-YSZ, Δ-YSZ polymorphs in the present work. Lattice parameters a, b and c are in Å, and crystalline angle α, β, and γ are in degrees.

	a	b	c	α	β	γ
c-ZrO_2	5.08	—	—	—	—	—
m-ZrO_2	5.17	5.19	5.33	—	99.36	—
Σ-YSZ	6.28	14.96	15.74	88.19	66.48	24.45
Ω-YSZ	6.40	6.19	6.30	99.96	100.75	98.57
Φ-YSZ	6.30	6.30	12.11	116.00	116.00	119.65
Δ-YSZ	6.37	6.28	6.48	81.53	99.59	99.98

3.1. Dielectric properties

In this work, the thermodynamically stable structures of YSZ at 10–40% mol Y_2O_3 composition with their stoichiometries are named as follows: (I) Σ-YSZ (14% mol yttria, $Zr_6Y_2O_{15}$), (II) Ω-YSZ (17% mol yttria, $Zr_5Y_2O_{13}$), (III) Φ-YSZ (20% mol yttria, $Zr_4Y_2O_{11}$), and (IV) Δ-YSZ (40 mol% yttria, $Zr_3Y_4O_{12}$). The relaxed lattice parameters are shown at table 1. Overall, these YSZ crystals are found to prefer triclinic symmetry. The fully relaxed crystalline geometries of these YSZ polymorphs are consistent with previous work [20, 23]. All of these YSZ phases are found to be insulators with finite electronic gaps (i.e. direct gaps): 4.06 eV (Σ-YSZ), 3.93 eV (Ω-YSZ), 4.14 eV (Φ-YSZ), and 4.20 eV (Δ-YSZ) [25], similar to the undoped zirconia, c-ZrO_2 and m-ZrO_2 (i.e. 3.58 eV and 3.83 eV respectively, in direct band gaps)[4].

The second derivatives of the total energy of these periodic solids with respect to collective displacements of the constituent atoms with different wavevectors commensurate with the underlying lattice are computed with variational density functional perturbation theory [7, 11–13]. One such property is the dielectric response of these materials. Compared to the reported experimental values [6] of YSZ dielectric constant, $\epsilon_0 \sim$ 10–41 from various morphologies, our computed ϵ_0 values fall within this range. Analogous to an amorphous-like (i.e. 96-atom supercell) [18] ZrO_2 (a-ZrO_2) solid, the dielectric tensor (i.e. ϵ_{ii}^{∞} and $\epsilon_{ii}^{\text{latt}}$ with $i = x, y, z$) of the low symmetry YSZ polymorphs are generally found to be rather isotropic and diagonal, irrespective of different

[4] It is well known that the LDA generally underestimate the band gaps, therefore without using the 'scissor-shift' to correct the electronic gap when calculating the electronic dielectric constants, we are expecting the LDA predicted ϵ^{∞} generally to be overestimated.

Table 2. Static dielectric constants of lattice contributions: $\epsilon^{\rm latt}_{xx}$, $\epsilon^{\rm latt}_{yy}$ and $\epsilon^{\rm latt}_{zz}$, and electronic contributions: ϵ^{∞}_{xx}, ϵ^{∞}_{yy} and ϵ^{∞}_{zz}, in three principal axes. The $\overline{\epsilon_0}$ is the sum of orientationally averaged $\overline{\epsilon^{\rm latt}}$ and $\overline{\epsilon^{\infty}}$ static dielectric constant.

System	ϵ^{∞}_{xx}	ϵ^{∞}_{yy}	ϵ^{∞}_{zz}	$\epsilon^{\rm latt}_{xx}$	$\epsilon^{\rm latt}_{yy}$	$\epsilon^{\rm latt}_{zz}$	$\overline{\epsilon_0}$
c-ZrO_2	6.05	6.05	6.05	40.58	40.58	40.58	46.63
m-ZrO_2	5.63	5.63	5.23	22.75	20.04	16.51	25.27
a-ZrO_2 [18]	4.76	4.62	4.54	20.30	17.10	15.50	22.27
Σ-YSZ	5.41	5.34	5.32	29.81	26.91	29.60	34.13
Ω-YSZ	5.25	5.28	5.29	20.40	20.51	20.20	25.64
Φ-YSZ	5.10	5.13	5.31	19.48	20.03	21.81	25.62
Δ-YSZ	4.81	4.77	4.68	19.92	17.06	23.14	24.79

Y_2O_3 composition (table 2). The orientationally averaged electronic dielectric constants, $\overline{\epsilon^{\infty}}$, over this range of YSZ compositions fall comfortably between the two c-ZrO_2 and a-ZrO_2 pure phases [18], i.e. $\overline{\epsilon^{\infty}_{\text{a-ZrO}_2}} < \overline{\epsilon^{\infty}_{\rm YSZ}} < \overline{\epsilon^{\infty}_{\text{c-ZrO}_2}}$, irrespective of Y_2O_3 composition. For the lattice contribution to the dielectric constant, a similar trend is observed, with $\overline{\epsilon^{\rm latt}_{\text{a-ZrO}_2}} < \overline{\epsilon^{\rm latt}_{\rm YSZ}} < \overline{\epsilon^{\rm latt}_{\text{c-ZrO}_2}}$ for all Y_2O_3 compositions in this study. Consequently, one can safely conclude that the orientationally averaged static dielectric constant, $\overline{\epsilon_0}$ (i.e. sum of $\overline{\epsilon^{\infty}}$ and $\overline{\epsilon^{\rm latt}}$) of YSZ follows the same trend as either $\overline{\epsilon^{\infty}}$ or $\overline{\epsilon^{\rm latt}}$, with respect to c- and a-ZrO_2 phases. For the undoped ZrO_2 morphologies, $\epsilon^{\rm latt}$ and ϵ_0 are a strong function of crystal structure due to distinct cubic and non-cubic symmetries. The doped, YSZ crystals in this study are all of low symmetry. In contrast to ZrO_2, the ϵ_0 of YSZ appears to be only a function of yttria concentration in the solid. As the yttria concentration increased, the orientationally averaged static dielectric constant, $\overline{\epsilon_0}$ of YSZ is found generally to decrease (table 2). Ultimately as the yttria concentration increased, one expects that consistent with these calculation, the $\overline{\epsilon_0}$ of YSZ will approach the static dielectric constant of Y_2O_3 ($\epsilon_0 \sim$ 12–20) [26, 27].

To understand the origin of these lattice dielectric responses, one has to begin with the atomic Born effective charges [13, 28] on the constituent atoms (Z^*_i) in the system, which determine the dielectric tensor $\epsilon^0_{\alpha\beta} = \epsilon^{\infty}_{\alpha\beta} + \frac{4\pi e^2}{\Omega}\Sigma_i \frac{Z^*_{i\alpha} Z^*_{i\beta}}{\omega_i^2}$ with Ω being the crystal unit cell volume, and ω_i being the phonon frequencies of IR-active modes [13]. For the crystal's macroscopic polarization due to internal displacements of its constituent atoms, the calculated Z^*_i tensors of YSZ generally have no symmetry, and are dominated by the diagonal terms for most atoms. To present the Z^* data in a manageable way, figure 1 is a scatter plot of just the isotropic averages (i.e. one-third of the trace) of the atomic Z^* tensors sorted by atom type for the system. Overall, the sum of $\langle Z^*_i \rangle$ of all atoms in ZrO_2 and YSZ in each unit cell will vanish within numerical accuracy, obeying the charge neutrality sum rule [13]. For cubic ZrO_2, the enhanced lattice contribution to the dielectric response $\epsilon^{\rm latt}$ (table 2) can be traced partly to an increase in Z^* of the constituent cations (Zr) and anions (O) in the system, with respect to the other YSZ solids as shown in figure 1. For c-ZrO_2, the isotropic charge tensor yields $Z^*_{\rm Zr}$ and $Z^*_{\rm O}$ to be 5.75 and −2.88 respectively, compared to $\langle Z^*_{\rm Zr} \rangle = 5.31$, $\langle Z^*_{\rm O_1} \rangle = -2.70$, and $\langle Z^*_{\rm O_2} \rangle = -2.61$ in the anisotropic monoclinic phase. For all YSZ phases, different atomic coordination number generally yields different Zr* values in the system. The $\langle Z^*_{\rm Zr} \rangle$ fall in the range 5.04–5.59, and $\langle Z^*_{\rm Y} \rangle$ in the range 3.79–3.97, and all oxygen anions have $\langle Z^*_{\rm O} \rangle$ in the range −2.44 to −2.76 (figure 1). Overall, the Born effective charges in YSZ are larger in magnitude than the nominal ionic valences of the isolated ions (+4, +3 and −2 for Zr, Y and O). The anomalously large Z^* values might indicate that there is a strong dynamic charge transfer from the chemical bonds, as the bond length varies during the perturbed displacements, due to the nature of mixed ionic–covalent bonds [17, 29].

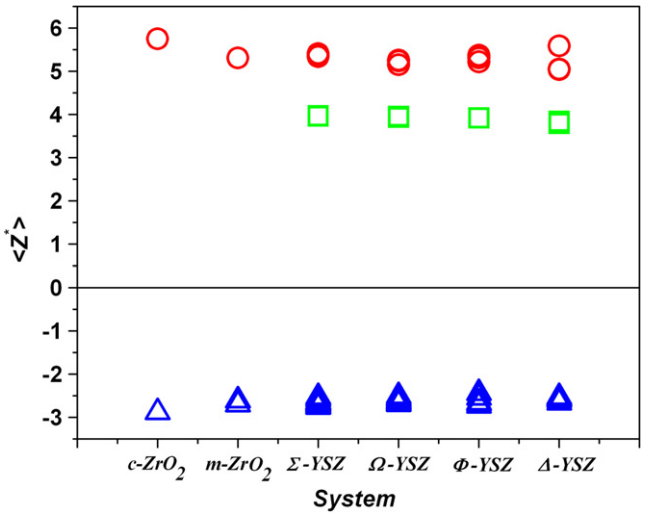

Figure 1. Scatter plot of isotropically averaged atomic Born effective charges, $\langle Z^* \rangle$ (vertical axis) for pure ZrO_2 (i.e. c-ZrO_2 and m-ZrO_2) and YSZ of various Y_2O_3 composition (Σ-YSZ: 14% mol yttria, Ω-YSZ: 17% mol yttria, Φ-YSZ: 20% mol yttria, and Δ-YSZ: 40 mol% yttria). Circles, squares, and triangles correspond, respectively, to Zr, Y, and O.

3.2. Thermodynamic properties

Of the relevant thermodynamic properties of YSZ, so far the only experimental data available is the heat capacity. In order to compare our theoretical results with these experimental findings, we focus on the heat capacity at constant volume, C_V of both ZrO_2 and the YSZ allotropes, obtained by linear response calculations based on the density functional perturbation theory [7, 11–13]. As a function of temperature derived from *ab initio* phonon band structures [30], the computed C_V of both ZrO_2 and YSZ are overall found comparable to the measured specific heat at constant pressure, C_P at low temperature [31, 32] (figure 2). As discussed in [32], the distinction between the two (i.e. C_P and C_V) for both ZrO_2 and YSZ is not significant at low temperature[5] [34].

[5] In general, the constant volume and constant pressure specific heats are related [33] by $C_P(T) - C_V(T) = E(T)T$, with $E(T) = \alpha_v^2(T) B V_{\rm mol}$ where $\alpha_v^2(T)$ is the temperature-dependent volume coefficient of thermal expansion, B is the bulk modulus, and $V_{\rm mol}$ is the molar volume at $T = 0$ K. The difference between C_P and C_V of both ZrO_2 and YSZ is significant only at high temperatures [34], and the correction factor can thus be negligible in our computed temperature range.

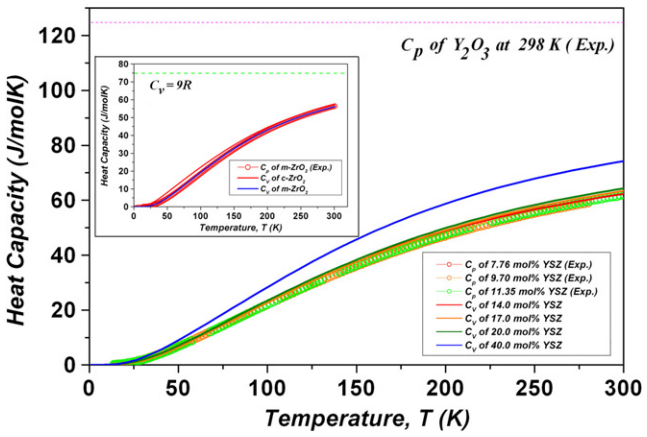

Figure 2. Experimental molar heat capacity [31, 32] (hollow circles) C_P of 7.76, 9.7 and 11.35 mol% YSZ together with the calculated specific heat (solid lines) C_V of Σ-, Ω, Φ, and Δ-YSZ, relative to the experimental C_P of Y_2O_3 (i.e. 102.51 J mol^{-1} K^{-1}) measured [35] at 298 K. Inset is both experimental [31] (hollow circle) and calculated (solid) heat capacities of zirconia solids: m-ZrO_2 and c-ZrO_2, relative to the green dotted horizontal classical asymptotic limit, $C_V = 9R$ (per formula unit, ZrO_2) which R is the universal gas constant, governed by the Dulong–Petit law.

Overall, the agreement between the computed value of m-ZrO_2 phase and the experimental data [31] is excellent (the inset of figure 2). At ∼300 K, our calculated C_V of m-ZrO_2 is 56.14 J mol^{-1} K^{-1}, compared to the experimental C_P value of 56.42 J mol^{-1} K^{-1}. Relative to the high temperature cubic phase, the heat capacity of the low temperature monoclinic phase is slightly lower. At elevated temperature, the two specific heats approach the classical asymptotic limit of 74.8 J mol^{-1} K^{-1}.

For the doped YSZ solids, the calculated heat capacities at room temperature are generally higher than the zirconia phases, but lower than yttria (Y_2O_3). At any finite temperature, the YSZ heat capacity will be bounded below by that of zirconia and above by that of yttria[6]. From the C_V values computed in this study, we found the C_V increased gradually as the yttria concentration increased. Thus, the heat capacity of YSZ (i.e. with x mol% yttria concentration) can be estimated quantitatively based on a simple additivity rule: $C_P^{\mathrm{YSZ}} = (1-x)C_P^{\mathrm{ZrO_2}} + xC_P^{\mathrm{Y_2O_3}}$, where $C_P^{\mathrm{ZrO_2}}$ and $C_P^{\mathrm{Y_2O_3}}$ are the heat capacity of pure zirconia and yttria, respectively [31]. Based on the experimental C_P values of pure zirconia and yttria solid at 298 K, the remaining difference between computed and interpolated values (i.e. ∼1.3–2.7%) for these YSZ solids, might be attributed to the small variances of lattice vibrational contribution during the solid state reaction between these two constituent compounds following the assumption of the Neumann–Kopp rule [35].

From the dynamical matrices obtained, the interpolation of force constants gives us the dispersion relations and density of states (DOS) of phonons shown in figure 3. All the zirconia and YSZ crystal structures that we obtained in this study are stable with respect to atomic vibration at the zone-center, the Γ-point. However, instabilities located elsewhere in the BZ are found for two crystals. For c-ZrO_2, the unstable phonon mode (i.e. ∼197i cm^{-1}) at X-point of the cubic zone boundary is consistent with the recent findings [16], which can be related to a stable zone-center A_{1g} phonon in the tetragonal form of zirconia. For the Σ-YSZ phase, the origins of the instability of multiple phonon modes (i.e. ∼436i–50i cm^{-1}) at the center along Γ–B are dominated by the phonon states from Zr and Y atoms in the solid.

Overall, the phonon distribution of both ZrO_2 and YSZ solids are very similar. All the phonon frequencies are below 800 cm^{-1} suggesting that O–O coupling does not occur in these solids. From the calculated phonon eigenvectors of these solids, the similarity of phonon states among the m-ZrO_2 and YSZ are found. At low frequencies (i.e. ∼ below 200 cm^{-1}), the phonon states are predominantly heavy cation motion (i.e. Zr in m-ZrO_2, Zr and Y in YSZ). While for high frequencies regime (i.e. ∼ above 600 cm^{-1}), the vibration contributions are mostly due to the coupling of Zr–O in the compounds. In addition, to further justify their similarity in phonon properties, specifically, we studied their average phonon frequencies[7], $\overline{\omega}$. For pure zirconia, the $\overline{\omega}_{\mathrm{ZrO_2}}$ ∼ 318–336 cm^{-1} at T = 300 K. Whereas for YSZ, $\overline{\omega}_{\mathrm{YSZ}}$ are 302–327 cm^{-1}. The similarity of $\overline{\omega}$ might be attributed to their similar phonon DOS within the linear responses regime. Most importantly, we find no gaps in the phonon DOS in c-, m-ZrO_2 and the YSZ solids in this study (figure 3). Despite these similarities, small deviations, however, can be found in both phonon dispersion and DOS between the c-ZrO_2 and YSZ: c-ZrO_2 phonon bands are more disperse with a significant high peak of phonon states around 200 cm^{-1}, whereas YSZ has more uniformly distributed phonon states due to flat dispersion. This suggests that the lattices of the later might be more rigid than the undoped zirconia.

4. Summary

In conclusion, we have calculated both the lattice dielectric and thermodynamic properties of yttria stabilized zirconia (YSZ) as a function of yttria concentration from phonon band structures based on density functional perturbation theory. Within the harmonic approximation, we find excellent agreement between our calculated specific heat and dielectric constants and low temperature experimental values. At 0 K, the density functional perturbation theory predicts that the dielectric constants of YSZ (i.e. ⩽40 mol% Y_2O_3) all fall between the amorphous and cubic zirconia. For zirconia, the static dielectric constant is found to be strongly influenced by system structural configurations. Whereas for YSZ, the static dielectric constant appears to be a function of yttria concentration in the solid. Overall, all the atomic Born effective charges which determine the lattice dielectric

[6] As the number of atoms in YSZ (i.e. $(ZrO_2)_{1-x}(Y_2O_3)_x$) varies with x, the normalized heat capacity $C_V = \frac{(3+2x)C_V^*}{N}$ (x = 0.14, 0.17, 0.20 and 0.40) is used throughout this paper, where C_V^* is the computed heat capacity, which proportional to number (N) of atoms in a unit cell.

[7] The average frequency is defined to be $\overline{\omega} = \sum_{i,q} \frac{C_{V(i,q)}\,\omega_{(i,q)}}{C_V}$, where $\omega_{(i,q)}$ is the frequency of the ith mode for q-point q, C_V is specific heat, and $C_{V(i,q)}$ is the contribution to the specific heat of the ith mode for q-point q as implemented in ABINIT program.

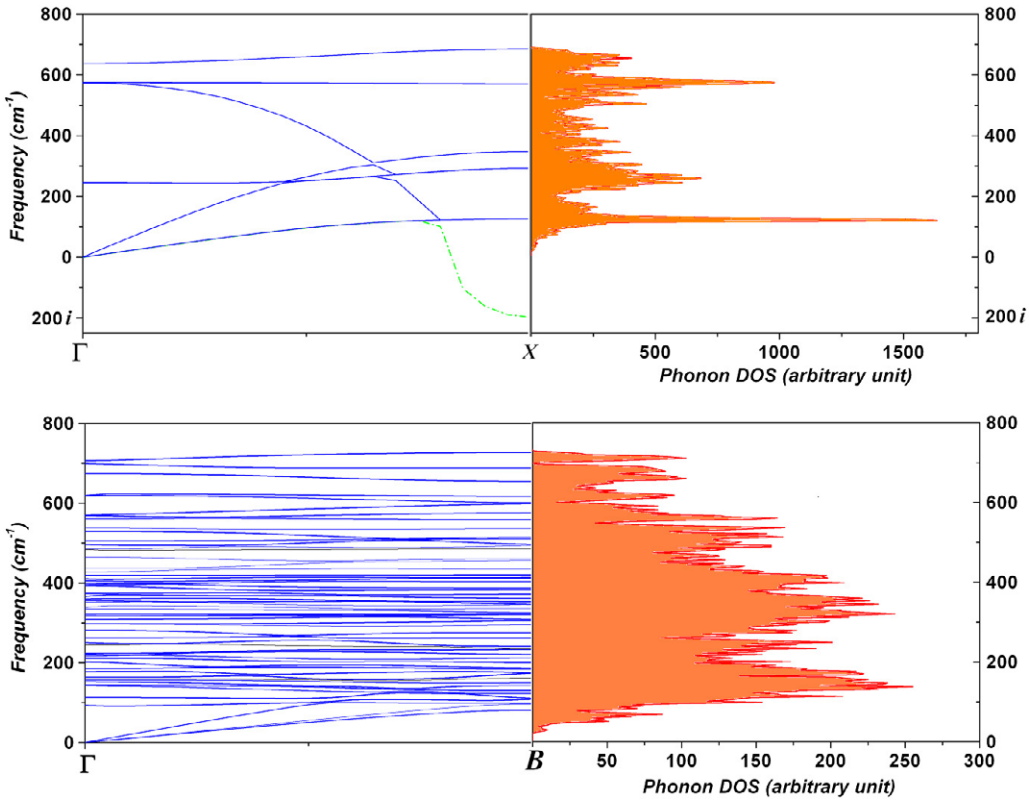

Figure 3. Phonon dispersion relation and density of states in c-ZrO_2 (top), and Δ-YSZ (bottom) in this study. The dotted green lines correspond to imaginary frequencies.

responses, are in general larger than the nominal ionic valences of the isolated constituent ions of the system. From the trend of specific heat of YSZ over different yttria composition, we suggest that the simple additivity rule can be a good approximation to quantitatively predict how the specific heat of a YSZ crystal depends on its yttria concentration. To gain further insight behind the mechanism of the excess heat capacity and at high temperature regime, clearly a systematic future study beyond linear responses regime is necessary. Ultimately this work can be used as baseline study to translate elementary electric and thermal responses, with respected to the ionic conductivity of YSZ solids and its interfaces into atomistic simulations of a working SOFC pertinent to experimental operating conditions.

Acknowledgments

We thank Dr Christopher R Ashman and the Naval Research Laboratory's High Performance Computing Project Investment Center for help with installing and using the ABINIT code and for a large amount of computer time. The Office of Naval Research, directly and through the Naval Research Laboratory supported this research.

References

[1] Kilner J A 2008 *Nat. Mater.* **7** 838
[2] Stapper G, Bernasconi M, Nicoloso N and Parrinello M 1999 *Phys. Rev.* B **59** 797
[3] Krishnamurthy R, Yoon Y, Srolovitz D and Car R 2004 *J. Am. Ceram. Soc.* **87** 1821
[4] Jamnik J and Maier J 1999 *J. Electrochem. Soc.* **146** 4183
[5] Lau K C, Turner C H and Dunlap B I 2008 *Solid State Ion.* **179** 1912
[6] Samara G A 1990 *J. Appl. Phys.* **68** 4214
Henn F E G, Buchanan R M, Jiang N and Stevenson D A 1995 *Appl. Phys.* A **60** 515
Hartmanova M, Gmucova K and Thurzo I 2000 *Solid State Ion.* **130** 105
Hendriks M G H M, ten Elshof J E, Bouwmeester H J M and Verweij H 2002 *Solid State Ion.* **146** 211
Vasco E and Zaldo C 2003 *Mater. Sci. Semicond. Process.* **5** 183
Jeong S H, Bae I S, Shin Y S, Lee S B, Kwak H T and Boo J H 2005 *Thin Solid Films* **475** 354
Zhu J and Liu J G 2003 *Mater. Lett.* **57** 4297
[7] Baroni S, Gironcoli S, Corso A D and Giannozzi P 2001 *Rev. Mod. Phys.* **73** 515
[8] Gonze X, Beuken J M, Caracas R, Detraux F, Fuchs M, Rignanese G M, Sindic L, Verstraete M, Zerah G, Jollet F, Torrent M, Roy A, Mikami M, Ghosez Ph, Raty J Y and Allan D C 2002 *Comput. Mater. Sci.* **25** 478 http://www.abinit.org
[9] Hartwigsen C, Goedecker S and Hutter J 1998 *Phys. Rev.* B **58** 3641
[10] Monkhorst H J and Pack J D 1976 *Phys. Rev.* B **13** 5188
[11] Gonze X, Allan D C and Teter M P 1992 *Phys. Rev. Lett.* **68** 3603
[12] Gonze X 1997 *Phys. Rev.* B **55** 10337
[13] Gonze X and Lee C 1997 *Phys. Rev.* B **55** 10355
[14] Jomard G, Petit T, Pasturel A, Magaud L, Kresse G and Hafner J 1999 *Phys. Rev.* B **59** 4044
[15] Christensen A and Carter E A 1998 *Phys. Rev.* B **58** 8050
[16] Rignanese G M, Detraux F, Gonze X and Pasquarello A 2001 *Phys. Rev.* B **64** 134301

[17] Zhao X and Vanderbilt D 2002 *Phys. Rev.* B **65** 075105
[18] Zhao X, Ceresoli D and Vanderbilt D 2005 *Phys. Rev.* B **71** 085107
[19] Dash L K, Vast N, Baranek P, Cheynet M C and Reining L 2004 *Phys. Rev.* B **70** 245116
[20] Bogicevic A, Wolverton C, Crosbie G M and Stechel E B 2001 *Phys. Rev.* B **64** 014106
[21] Ostanin S, Salamatov E, Craven A J, McComb D W and Vlachos D 2002 *Phys. Rev.* B **66** 132105
[22] Ostanin S and Salamatov E 2003 *Phys. Rev.* B **68** 172106
[23] Predith A, Ceder G, Wolverton C, Persson K and Mueller T 2008 *Phys. Rev.* B **77** 144104
[24] Raczkowski D, Fong C Y and Stechel E B 2004 *Modelling Simul. Mater. Sci. Eng.* **12** 133
[25] Lau K C and Dunlap B I 2008 unpublished results
[26] Andreeva A F, Sisonyuk A G and Himich E G 1994 *Phys. Status Solidi* a **145** 441
[27] Wilk G D, Wallace R M and Anthony J M 2001 *J. Appl. Phys.* **89** 5243
[28] Ghosez Ph, Michenaud J P and Gonze X 1998 *Phys. Rev.* B **58** 6224
[29] Zhong W, King-Smith R D and Vanderbilt D 1994 *Phys. Rev. Lett.* **72** 3618
[30] Lee C and Gonze X 1995 *Phys. Rev.* B **51** 8610
[31] Tojo T, Atake T, Mori T and Yamamura H 1999 *J. Chem. Thermodyn.* **31** 831
[32] Tojo T, Atake T, Mori T and Yamamura H 1999 *J. Therm. Anal. Calorim.* **57** 447
[33] Ashcroft N W and Mermin N D 1976 *Solid State Phys.* (Philadelphia, PA: Saunders)
[34] Degueldre C, Tissot P, Lartigue H and Pouchon M 2003 *Thermochim. Acta* **403** 267
[35] Leitner J, Chuchvalec P, Sedmidubský D, Strejc A and Abrman P 2003 *Thermochim. Acta* **395** 27